APPLICATIONS OF COMPUTATIONAL SCIENCE AND ENGINEERING TO MOLTEN SLAG AND RELATED ISSUES IN STEELMAKING

Tooru Matsumiya
Nippon Steel Corporation, Japan

ABSTRACT

Firstly, optimization of demanganezation process of hot metal and mold flux design in continuous casting by the use of coupled reaction model and its modification are mentioned. Secondly, chemical composition control of nonmetallic inclusions is shown by the use of coupled precipitation model, which was developed by the present author. The model is explained and its application to an austenitic stainless steel for wire drawing is introduced. Since the cell model is widely used as thermodynamic model for slag and flux in Nippon Steel Corporation, a newly proposed evaluation method of energy parameter values in the cell model is discussed thirdly. Then, the molecular dynamic simulation of $CaO\text{-}SiO_2$ *melts is carried out for estimation of the diffusion coefficients of every ions in the melts and their silicate structure. Finally, the estimation of thermodynamic properties of solutes in silicon melts by the use of first-principle calculation is mentioned which can be applied to slag and flux systems in the future.*

INTRODUCTION

Ranging from continuum mechanics to electronic structure analysis, phenomenological simulation and atomistic simulations in between, various computational science and engineering is applied to molten slag related issues in steelmaking. They are both for optimization of processes and basic understanding of slag properties and structure which should be known in the process simulations. In this paper some of their examples in Nippon Steel Corporation are presented.

OPTIMIZATION OF DEMANGANIZATION PROCESS

The refining of steel is conducted mainly by the use of slag/metal reaction and injection metallurgy. In both cases chemical reaction occurs between liquid metal and refining agents that are frequently liquid oxides. The slag/metal refining process can be analyzed by coupled reaction model [1]. The reaction between injected flux and metal can be analyzed in the same manner. This model was applied to optimize demanganization process of hot metal, where iron oxide powder is injected in a hot metal through an immersed nozzle [2]. The chemical composition change of the injected powder is analyzed with the model. The results are shown in Figure 1. Silica concentration in the injected powder increases and iron oxide concentration decreases monotonically, while manganese oxide concentration reaches its maximum and decreases as time elapses after the powder is injected. This is because oxygen potential in the powder is not high enough to oxidize manganese in hot metal after the manganese oxide content reaches its maximum and manganese oxide is reduced back to hot metal. Therefore, from the viewpoint of efficient demanganization the injected powder is desired to float up to the top slag when the manganese concentration in the powder reaches the maximum. Since the time at the maximum manganese concentration becomes longer as demanganization process proceeds due to less concentration of silicon and manganese in hot metal, the depth of nozzle immersion should be increased accordingly to realize efficient demanganization. Based on this finding, the demanganization process is operated successfully.

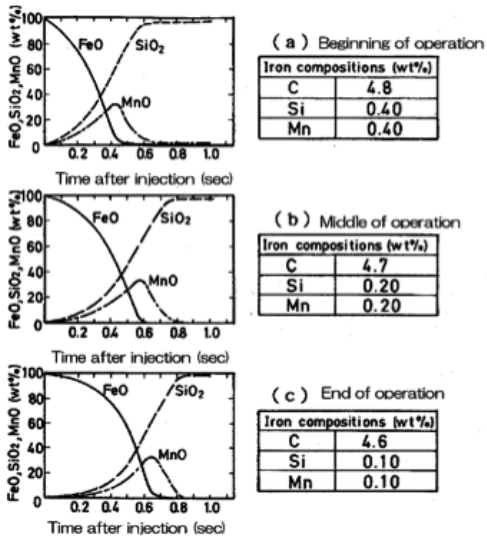

Figure 1: Chemical composition changes in the refining powder after the injection to hot metal in demanganization and desiliconization process

MOLD FLUX DESIGN IN CONTINUOUS CASTING

In the continuous casting mold flux is applied for the lubrication between the casting and the mold. Although the chemical compositions of the mold flux is optimized for this purpose, the behavior changes due to its chemical composition change during the casting through the reaction with the liquid metal. The chemical composition change because of the reaction was analyzed by the use of the coupled reaction model [3]. Since the fresh mold flux is added from the top and the reacted flux flows out through the mold-casting gap and fresh molten metal is powered through submerged entry nozzle to the mold and the reacted metal goes out the mold, the mass balance of every chemical substances in both the flux and the metal due to these material flows are included into the input and output associated to the chemical reaction between metal and flux at their interface. Figures 2 and 3 show the calculated chemical compositions change in the flux pool during the casting of Ti-contained steel, the chemical compositions of which is listed in Table 1. The initial chemical compositions of the fluxes are listed in Table 2. In the case of flux with higher CaO/SiO_2 ratio the TiO_2 content increases much as shown in Figure 2 and CaO/TiO_2 precipitates, which causes sticking of initial solid to the mold. On the other hand in the case of flux with low CaO/SiO_2 ratio the increment of TiO_2 is not significant (Figure 3), which is because the TiO_2 activity is high (Figure 4) and concomitantly the diffusion of TiO_2 to the flux is discouraged, and CaO/TiO_2 does not precipitate. By the use of this analysis mold flux can be designed beforehand with the consideration of its chemical composition change during the casting by the reaction.

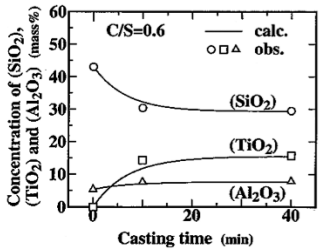

Figure 2: Comparison of calculated composition change of mold flux during continuous casting of high titanium steel with observed one

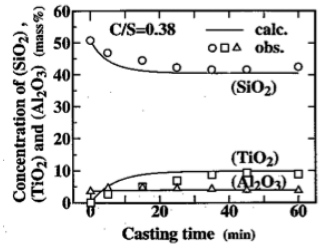

Figure 3: Comparison between calculated composition changes of mold flux and observed one for C/S of 0.38

Table 1: Chemical composition of steel (mass%)

C	Si	Mn	Al	Ti	O
0,03	0,34	0,34	0,044	0,33	0,0015

Table 2: Chemical compositions of mold fluxes (mass%)

	CaO	SiO_2	Al_2O_3	Na_2O	CaF_2
A	26	43	5	12	14
B	19	51	4	13	13

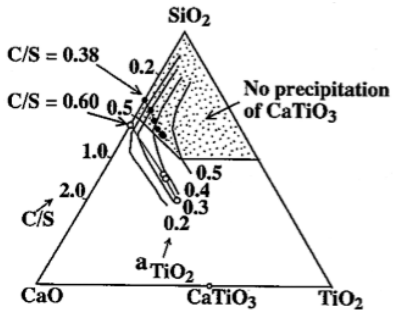

Figure 4: Estimated iso-activity lines of TiO_2 in mold flux and change in composition of mold flux for high titanium steel on CaO-SiO_2-TiO_2 quasi-ternary phase diagram

CHEMICAL COMPOSITION CONTROL OF NONMETALLIC INCLUSIONS

Coupled Precipitation Model

Coupled precipitation model [4] was developed to analyze chemical composition change of nonmetallic inclusions during solidification of steels. Basic equations are as follows:

$$(1-k^i)C_L^i df_S=\{1-(1-2\Omega^i k^i)\, f_S\}\, dC_L^i+\Sigma_j Rp_{ij} dP_j \quad (1)$$

Where super suffix i indicates the kind of solute, k^i is equilibrium partition coefficient, C_L^i is solute concentration in liquid, df_S is fraction solid, Ω^i is modified solidification parameter, Rp_{ij} are moles of element i in the precipitate j and P_j is concentration of precipitate j. If the last term in Equation (1) is omitted, integration of which gives equation of solidification microsegregation proposed by Clyne and Kurz [5]. Equation (1) is solved with mass action equation of precipitation:

$$\Pi_i a_i R^{pij}/aj=K_j \quad (2)$$

where ai is activity of element i, a_j is activity of precipitate j and K_j is the equilibrium constant of precipitate j. That is, in the coupled precipitation model solidification microsegregation is analysed with consideration of back diffusion of solutes into solid and local thermodynamic equilibrium is assumed in the residual liquid including the precipitation of non-metallic inclusions (Figure 5).

Oxide Inclusion Control in Austenitic Stainless Steel for Wire Drawing

The inclusions in an austenitic stainless steel for wire drawing should be deformable during the wire hot rolling. Other wise wire breaking occurs at the hard crystalline phases in the inclusions during the process. The coupled precipitation model was applied to con-

trol the oxides inclusions in this steel whose chemical compositions are listed in Table 3 [6]. Figure 6 shows the calculated Al_2O_3 and SiO_2 concentrations as functions of fraction solid and total oxygen content in the steel by the use of coupled precipitation model. The calculated concentrations at the fraction solid of 0.5 agree well with the experimentally observed ones. The increase of total oxygen content from 40 ppm to 80 ppm sharply decreases Al_2O_3 concentration and sharply increases SiO_2 concentration, which may change the nature of the oxide inclusions. However, further increase of total oxygen does not change so much Al_2O_3 and SiO_2 concentrations, that is, the nature of inclusions. The increase only increases the amount of inclusions.

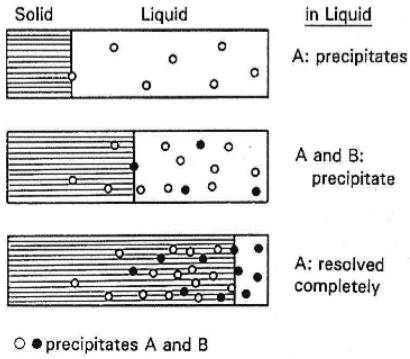

Figure 5: Schematic diagram of the coupled reaction model

Table 3: Chemical compositions of the austenitic stainless steel in mass%

Cr	Ni	C	Si	Mn	Al
18,3	10,35	0,02	0,5	1,1	0.0015-0.0030
	O	Mo		Ca	Mg
	0.0040 _ 0.0150	0,01		0,0005	0,0004

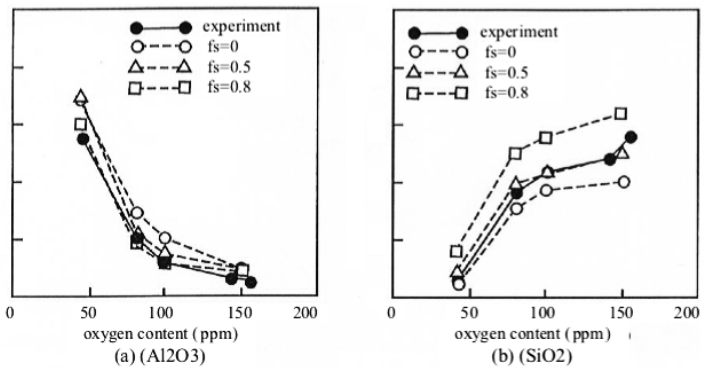

Figure 6: Alumina and silica contents in inclusions as functions of total oxygen content

By the use of thermodynamic equilibrium calculation the liquidus temperature of inclusions and fractions of various crystalline phases appeared in the inclusions at the various temperature can be obtained [6]. Figure 7 compares the calculated fractions of each phase in oxide inclusions at various temperatures in the stainless steels with total oxygen

content of 40 ppm and 80 ppm. In the inclusions in the steel with total oxygen content of 40 ppm, hard crystalline phases such as Al_2O_3 and spinnel $MgO{\cdot}Al_2O_3$ occupy large portion even at high temperature of 1600°C. These inclusions are considered to be undeformable. On the other hand, in the inclusions in the steel with oxygen content of 80 ppm, liquid phase occupies 80% even at the low temperature of 1200°C. These inclusions are considered to be deformable. According to this finding an austenitic stainless steel for wire drawing was successfully developed.

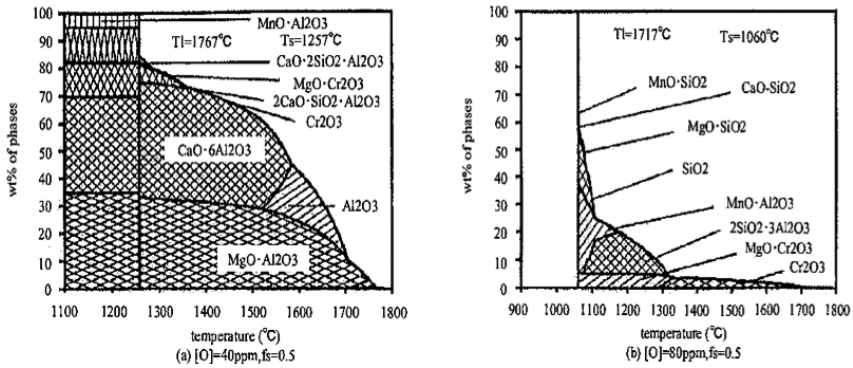

Figure 7: Calculated fractions of various phases in inclusions at various temperatures

EVALUATION OF PARAMETER VALUES IN CELL MODEL FOR SLAG THERMODYNAMICS BY NMR

Thermodynamic models describe free energy of each phase as a function of its composition, temperature and pressure and are used for the equilibrium calculation of multicomponent system at a given temperature, pressure and total compositions of the system. The cell model is one of a prominent thermodynamic model for slags and fluxes [7]. In this model the number of each cell R_{ij} in liquid oxide solutions, which consists of cation pair and an oxygen atom in between, is calculated so that the free energy of the solutions is minimized under a condition of the set values of the energy parameters, formation enthalpy of cells with heterogeneous cation pairs W_{ij} and interaction energy between cells E_{ij}, with consideration of the entropy of mixing of the cells. The energy parameters are mainly accessed by the comparison of the calculated phase boundaries of multi-component liquid slags and precipitating solid phases, and sulfide and phosphate capacities of slags by using the cell model for slags with observed ones. These values come from the result of equilibrium between slags and others, which are solid oxides and liquid steels. Therefore, if some evaluated values of the others are changed, the accessed energy parameters of slag must be re-assessed in order to satisfy the equilibrium relation with them.

On the other hand, since the chemical shift in nuclear magnetic resonance (NMR) spectrum of oxygen varies depending on what kinds of cations sit in both side of the oxygen, the relative number of each kind of cell can be measured from the intensity of the peak, which corresponds to the cell, in the oxygen NMR spectra. The present author, et al. proposed to evaluate the energy parameters values in the cell model more directly so that the calculated fraction of each cell in a slag at its minimum free energy state agrees the measured fraction by NMR spectra, in order to overcome the drawback in the rather indirect evaluation method of the parameters mentioned above [8].

Calculation of BO/NBO Ratio in Al_2O_3-CaO-SiO_2 Slag by Cell Model

The chemical compositions of test slags are listed Table 4. The moles of various cells in the slags were calculated by using the cell model with energy parameters listed in Table 5, which are the same ones in the original cell model. The calculated moles are listed in Table 6. Since the slag alumina content is less than the composition of 'tectosilicate', where the charge of the modifier cation equals to aluminum atoms, aluminum atoms are in the silicate network [9], where oxygen in the cell (Al-O-Ca) had better be counted as bridging oxygen. Therefore, the BO/NBO ratios in slag A, B and C derived from Table 6 are approximately 42.5/57.5, 45/55 and 70/30, respectively.

Table 4: Chemical composition of slags

Slag	SiO_2	Al_2O_3	CaO
A	34.9mass% (0.360mol)	16.2mass% (0.099mol)	48.9mass% (0.541mol)
B	38.23mass% (0.395mol)	15.68mass% (0.095mol)	46.08mass% (0.510mol)
C	57.4mass% (0.601mol)	15.9mass% (0.098mol)	26.8mass% (0.301mol)

Table 5: Parameter values (cal/mol) (W^k_{ij} and E^k_{ij} are indicated as W(i-k-J) and E(i-k-j), respectively)

W(Si-O-Al) = 2000	E(Si-O-Al) = -3000
W(Si-O-Ca) = -12500	E(Si-O-Ca)= -4500+7500X(SiO2)
W(Al-O-Ca) = -8500+3000X(Al_2O_3)	E(Al-O-Ca) = -5500-5000X(Al_2O_3)

Table 6: Calculated moles of various cells (moles and molar fractions)

slag	(Si-O-Si)	(Al-O-Al)	(Si-O-Al)	(Ca-O-Ca)	(Si-O-Ca)	(Al-O-Ca)	Total mole
A	0,228 (0,146)	0,158 (0,101)	0,092 (0,059)	0,002 (0,001)	0,894 (0,574)	0,184 (0,118)	1,558 (1,000)
B	0,300 (0,189)	0,160 (0,101)	0,107 (0,067)	0,001 (0,001)	0,871 (0,550)	0,146 (0,092)	1,586 (1,000)
C	0,803 (0,447)	0,153 (0,075)	0,258 (0,143)	0,000 (0.000)	0,54 (0,301)	0,061 (0,034)	1,797 (1,000)

NMR Measurements of BO/NBO Ratio in Al_2O_3-CaO-SiO_2 Slags

^{17}OMAS spectrum and ^{27}Al→ ^{17}O CP/MAS spectrum of the slag with same composition as test slag B full labeled and calcinated at 1400°C were measured. The results are shown in Figure 8. Since the peak in ^{27}Al→ ^{17}O CP/MAS spectrum can be assigned as BO peak, the other peak in ^{17}OMAS spectrum is assigned as NBO peak. From the relative intensities of these peaks in ^{17}OMAS spectrum the BO/NBO ratio is measured to be approximately 42/58. ^{17}OMAS spectrum of slags with compositions of slags A and C full labeled and calcinated at 1400°C were also measured. From the relative intensities of these peaks in ^{17}OMAS spectrum the BO/NBO ratios in slags A and C are measured to be approximately 48.5/51.5 and 76/24, respectively.

Although the moles of every cells could not be separately measured by NMR at this moment, the BO/NBO ratio measured by NMR is in good agreement of the calculated one by the cell model with already assessed energy parameters. It means that NMR results also support the energy parameter values assessed before by the *indirect* method and that the *direct* evaluation method proposed here has possibility in its validity.

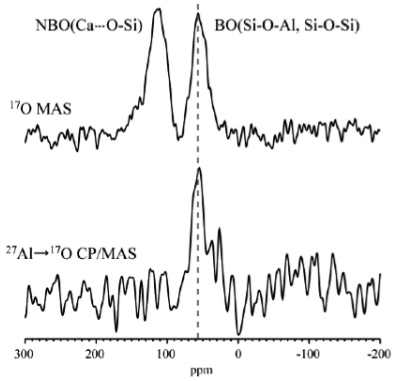

Figure 8: ^{17}O MAS spectra and $^{27}Al \rightarrow {}^{17}O$ CP/MAS spectra of slag B

MOLECULAR DYNAMICS SIMULATION OF $CaO\text{-}SiO_2$ SLAGS

Diffusion coefficients of Ca, Si and O ions were obtained by molecular dynamics simulation of molten $CaO\text{-}SiO_2$ slag [10]. Born-Mayer-Higgins inter-atomic potentials are used in the simulation. Parameter values in the inter-atomic potentials are obtained by the use of the experimental data of cohesive energy, nearest neighbor distance, etc. By assuming random walk of atoms the gradient of the plots of mean square displacement of atom vs. elapsed time gives 1/6D where D is diffusion coefficient of the atom. Figure 9 summarized calculated diffusion coefficients of Ca, Si and O ions as functions of CaO concentration in the slags, which agree well with the reported experimental values. Simultaneously, slag structure was obtained which can be utilized for evaluation of cell model for thermodynamics. Figure 10 shows the fractions of silicon ions with various number of non-bridging oxygen ions as functions of CaO concentration. The calculated behaviors are in agreement with observation [11].

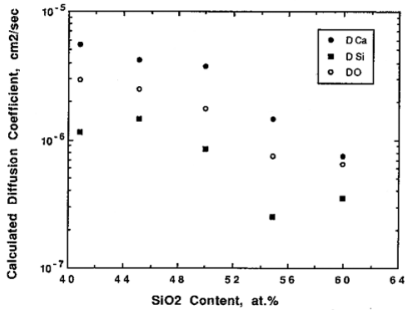

Figure 9: Calculated diffusion coefficients of Ca, Si and O ions in $CaO\text{-}SiO_2$ melts as functions of CaO content at 1873K

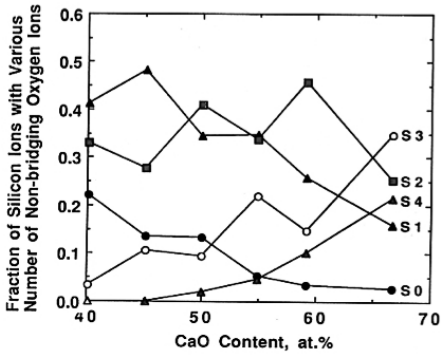

Figure 10: Calculated fractions of silicon ions with various numbers of non-bridging oxygen ions as functions of CaO content in CaO-SiO_2 melts

ABINITIO CALCULATION OF THERMODYNAMIC PROPERTIES

Ab initio calculation was applied to estimate thermodynamic properties of solute element in silicon [12]. From energy difference of solute X in silicon at dilute solution condition and solute element in its standard state, that is, at its pure state Ω_{MX} activity coefficient of the solute γ^0_x can be derived as follows:

$$RT \ln \gamma^0_x = \Omega_{MX} \tag{3}$$

Ω_{MX} can be efficiently calculated in solid state by electronic band calculation since small calculation cell size can be used because of the periodicity of atomic configuration in crystal. The obtained activity coefficient in solid silicon is converted to that in liquid silicon, whose experimental value is available, based on the following relation.

$$\mu^0_x(L) + RT \ln\gamma^0_x(L)X(L) = \mu^0_x(S) + RT \ln\gamma^0_x(S)X(S) \tag{4}$$

$$RT \ln\gamma^0_x(L) = RT \ln\gamma^0_x(S) + \ln X(S)/X(L) + (\mu^0_x(S) - \mu^0_x(L))/RT \tag{5}$$

$$\mu^0_x(S) - \mu^0_x(L) = \Delta S_s\ (Tm - T) \tag{6}$$

where, $\mu^0_x(L)$ and $\mu^0_x(S)$ are free energy of solute X at pure liquid X and pure solid X, respectively, $\gamma^0_x(L)$ and $\gamma^0_x(S)$ are activity coefficient of solute X in liquid and solid infinite dilute silicon solution, respectively, and X(L) and X(S) are solute X concentrations in liquid and solid silicon, respectively. ΔS_s is the entropy of solidification and T_m is melting temperature of solute X. The calculated activity coefficient values are summarized in Figure 11 with comparison of reported experimental values [13, 14]. Relative values of calculated activity coefficients among Fe, Al and Ti are in agreement with experimental values, but calculated values are much higher than experimental ones by several orders. This is due to the X(S)/X(L) values, solid/liquid partition coefficient of solutes, k_x, applied in Equation (5) was those near the melting points of silicon. It is considered that $\gamma^0_x(S)$ is icreaced much faster than $\gamma^0_x(L)$ as the temperature goes down since the solid phase becomes much stiffer in comparison to the under cooled liquid phase and solubility of X becomes much smaller in solid than in liquid at the low temperature. Therefore, the kx is much smaller at 0K than at the melting temperature of silicon. Since calculation of $\gamma^0_x(S)$,

that is Ω_{MX}, is done at 0K, much smaller values for X(S)/X(L) should have been used for conversion of $\gamma^0{}_x$ (S) into $\gamma^0{}_x$ (L) in Equation (5).

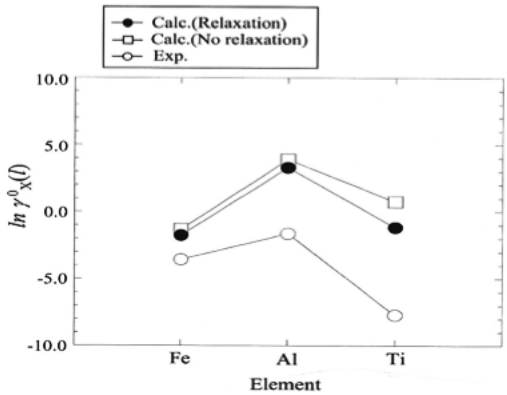

Figure 11: Comparison of calculated activity coefficients with experimental values at the temperature of 1723K

This kind of ab-initio calculation can be also utilized in estimation of thermodynamic properties of molten slag and evaluation of inter atomic potentials which are used in molecular dynamics simulation of slag.

REFERENCES

Robertson, D. G. C., Deo, B. & Oguchi, S. (1984). *Muticomponent Mixed-Transport-Control Theory for Kinetics of Coupled Slag/Metal and Slag/Metal/Gas Reactions: Application to Desulphurization of Molten Iron*. Ironmaking and Steelmaking, 11(1), pp. 41-55. [1]

Kitamura, T., Shibata, K., Sawada, I. & Kitamura, S. (1989). *Optimization of Refining Process by Computer Simulation*. Bulletin of Japanese Institute of Metals, 28(4), pp. 310-312 (in Japanese). [2]

Kiyose, A., Miyazawa, K., Yamada, W., Watanabe, K. & Takahashi, H. (1996). *Mathematical Modelling of Change in Composition of Mold Flux in Continuous Casting of Steels*. ISIJ Int., 36(Supplement), pp. S155-S158. [3]

Matsumiya, T. (1992). *Mathematical Analyses of Segregations and Chemical Compositional Changes of Nonmetallic Inclusions during Solidification of Steels*. Trans JIM, 33(9), pp. 783-794. [4]

Clyine, T. W. & Kurz, W. (1981). *Solute Redistribution during Solidification with Rapid Solid State Diffusion*. Metall. Trans. A, 12A(6), pp. 965-971. [5]

Yamada, W., Matsumiya, T., Fukumoto, S., Tanaka, S. & Takeuchi, H. (1993). *Simulation of the Compositions of Nonmetallic Inclusions in Cast Stainless Steels*. Proceedings of Intern Conf on Computer-assisted Materials Design and Process Simulation. Tokyo, ISIJ, pp. 123-128. [6]

Gaye, H. & Welfringer, J. (1984). *Modelling of the Thermodynamic Properties of Complex Metallurgical Slags*. Proc. 2nd Int. Sympo. on Metallurgical Slags and Flues, ed. H. A. Fine and D. R. Gaskell, TMS-AIME, Warrendale, P.A., pp. 357-375. [7]

Matsumiya, T., Shimoda, K., Saito, K., Kanehashi, K. & Yamada, W. (2007). *A Proposal for Evaluation Method of Energy Parameter Values in Cell Model for Thermodynamics of Refining Slag*. ISIJ-Int., 47(6), 2007, pp. 802-804. [8]

Mysen, B. O. (1988). *Structure and Properties of Silicate Melts*. Elsevier, Amsterdam, p. 80. [9]

Matsumiya, T., Nogami, A. & Fukuda, Y. (1993). *Applicability of Molecular Dynamics to Analyses of Refining Slags*. ISIJ-Int., 33(1), pp.210-217. [10]

Kashio, S. (1979). Master of Engineering Thesis , University of Tohoku. [11]

Iwata, K., Matsumiya, T., Sawada, H. & Kawakami, K. (2003). *Prediction of Thermodynamic Properties of Solute Elements in Si Solutions Using First-Principles Calculation*. Acta Materialla, 51(2), pp. 551-559. [12]

Miki, T., Morita, K. & Sano, N. (1997). *Thermodynamic Properties of Titanium and Iron in Molten Silicon*. Metall Mater Trans B, 22B(5), pp. 861-867. [13]

Miki, T., Morita, K. & Sano, N. (1999). *Thermodynamic Properties of Si-Al, -Ca, -Mg Binary and Si-Ca-Al, -Ti, -Fe Ternary Alloys*. Materials Trans JIM, 40(10), pp. 1108-1116. [14]